

# A biochemical machine for the interconversion of mutual information and work

Thomas McGrath,<sup>1</sup> Nick S. Jones,<sup>1</sup> Pieter Rein ten Wolde,<sup>2</sup> and Thomas E. Ouldridge<sup>1,\*</sup>

<sup>1</sup>*Department of Mathematics, Imperial College London, London, SW7 2AZ, UK*

<sup>2</sup>*FOM Institute AMOLF, Science Park 104, 1098 XE Amsterdam, The Netherlands*

(Dated: December 3, 2024)

We propose a physically-realisable biochemical device that is coupled to a biochemical reservoir of mutual information, fuel molecules and a chemical bath. Mutual information allows work to be done on the bath even when the fuel molecules appear to be in equilibrium; alternatively, mutual information can be created by driving from the fuel or the bath. The system exhibits diverse behaviour, including a regime in which the information, despite increasing during the reaction, enhances the extracted work. We further demonstrate that a modified device can function without the need for external manipulation, eliminating the need for a complex and potentially costly control.

From the spatial clustering of food molecules to cycles in temperature and sunlight over the course of a year, environmental correlations are exploited by biological systems. Generating correlations is also at the heart of information transmission, a process of great importance in biology [1]. Consequently, recent years have seen great interest in applying information theoretic approaches in the biological contexts of sensing [2–4], signalling [5, 6], adaption [7, 8], chemotaxis [9, 10] and more widely [11].

Simultaneously, the thermodynamic consequences of information have been explored [12–20]. Much work has focused on the “information entropy”,  $H(X) = -\sum_{x \in X} p(x) \ln p(x)$ , which quantifies the uncertainty present in the state of a system  $X$  [21–23]. Correlations, however, are quantified by the mutual information  $I(X; Y) = \sum_{x \in X, y \in Y} p(x, y) \ln \frac{p(x, y)}{p(x)p(y)}$ .  $I(X; Y)$  gives the degree to which knowledge of  $X$  reduces uncertainty about  $Y$ , and vice-versa. A central result, essential in exorcising Maxwell’s Demon [4, 24], is that correlations between systems  $X$  and  $Y$  that are currently non-interacting imply a non-equilibrium free energy [20, 25]

$$\tilde{F}(X, Y) = \tilde{F}(X) + \tilde{F}(Y) + k_B T I(X; Y). \quad (1)$$

Here,  $\tilde{F}(X) = F_{\text{eq}}(X) - kT \sum_{x \in X} p(x) \ln \frac{p_{\text{eq}}(x)}{p(x)}$  is the non-equilibrium free energy of a system  $X$  coupled to a heat bath at temperature  $T$  [20, 26]. Intuitively, if  $X$  and  $Y$  are not currently interacting, the true equilibrium should exhibit independence,  $I(X; Y) = 0$ . Any mutual information created by the history of  $X$  and  $Y$  implies that the overall system is currently out of equilibrium.

Eq. 1 shows that correlations can be exploited to extract work. We propose a simple and physically-realisable biochemical device that achieves such a feat, a basis for the development of more sophisticated information-exploiting systems. We present first a device inspired by the externally-manipulated, tape-driven machines introduced by Bennett [13], and studied in detail by Mandal, Jarzynski and others [21–23, 25, 27–30]. We

then show that the device can be modified to be truly autonomous, eliminating the need for external control, the costs of which are typically neglected. Other than in Ref. [30], previous designs do not inter-convert work and free energy stored in long-lived correlations of degrees of freedom external to the device. Moreover, for none of the designs previously analysed in detail (including Ref. [30] and also experimental measurement-feedback systems [31, 32]) is the physical information-processing mechanism made explicit – despite Landauer’s aphorism “Information is physical” [33]. By considering an implementation of an information processing device, we demonstrate the natural manner in which information is a thermodynamic resource; illustrate mechanisms by which information and work can be interconverted that permit the construction of actual machines; and emphasize the physical constraints that limit such systems.

Our device, explained below, is illustrated in Fig. 1 (a). At its heart is an enzyme  $E$ , which can be converted from inactive ( $E$ ) to active ( $E^\dagger$ ) by the allosteric binding of molecule  $Y$ . The enzyme can also bind to nucleotides ADP/ATP, and a substrate molecule  $X$ . When active,  $E^\dagger$  catalyses phosphate exchange between ATP and  $X$



One natural enzyme/substrate/activator combination would be LKB1, AMPK and STRAD-MO25 [34], although others exist [35] and engineered examples [36, 37] might provide optimal properties.

We set up the device with  $E$  tethered to a fixed point, within a bath of ATP and ADP, as shown in Fig. 1 (a) and (b). The enzyme itself is the engine. The nucleotide bath is a reservoir against which chemical work can be done. The free-energy changes associated with adding an ATP or ADP to solution are given by  $\mu_{\text{ATP}}$  and  $\mu_{\text{ADP}}$ , respectively. Converting ADP into ATP constitutes positive work output from the engine if the chemical potentials are such that  $\mu_{\text{ATP}} > \mu_{\text{ADP}}$ . The enzyme’s fuel is supplied in the form of two “tapes”,  $A$  and  $B$ . These tapes contain pairs of sites,  $A_n$  and  $B_n$ , at regular intervals. At each  $A_n$  is  $X$  or  $X^*$ ;  $B_n$  carries  $Y$  or an empty space  $\bar{Y}$ . The two tapes cannot move independently, and the inter-site interval is long enough that  $E$  can interact

\* t.ouldridge@imperial.ac.uk

with at most one pair of sites at any given time. The pairs  $A_n, B_n$  are initially independent of  $A_m, B_m$  for  $n \neq m$ .

An operational cycle begins with  $E$  isolated from the sites on either tape, and in equilibrium with respect to ATP/ADP binding from the bath. We then manipulate  $A$  and  $B$  externally to bring the next pair of sites,  $n$ , alongside  $E$ . If  $B_n = Y$ ,  $E \rightarrow E^\dagger$  and conversion of  $A_n$  between  $X$  and  $X^*$  according to Eq. 2 is possible.  $B_n$  remains unchanged during the interaction window – its state is quenched. We then move  $A$  and  $B$  on, allowing  $E$  to relax back into equilibrium with the chemical bath. We return to the costs of external manipulation later.

In the absence of tape  $B$ , and with a constitutively active enzyme, tape  $A$  is the only source of free energy with which to do work on the bath. This free energy depends on the intrinsic stabilities of  $X$  and  $X^*$ ,  $\mu_X$  and  $\mu_{X^*}$ , which give  $q_{\text{eq}} = p_{\text{eq}}(A_n = X^*) = (1 + \exp((\mu_{X^*} - \mu_X)/k_B T))^{-1}$  as the equilibrium fraction of  $X^*$ , and the initial probability  $q = p_0(A_n = X^*)$ . Specifically,  $\tilde{F}(A_n) - F_{\text{eq}}(A_n) = (q - q_{\text{eq}})(\mu_{X^*} - \mu_X) + k_B T(H_{\text{eq}}(A_n) - H(A_n))$ . Note that the free energy  $\tilde{F}(A_n)$  depends on the intrinsic stabilities of  $X$  and  $X^*$  in isolation from ATP and ADP. Relaxation to equilibrium via slow “spontaneous” transitions uncoupled from  $E$ , ADP and ATP minimize this free energy. These spontaneous transitions involve exchange of  $P_i$  directly with solution.

Thus tape  $A$  can be used to do work on the bath if it has an excess of the most unstable substrate, or a low entropy, or both. With  $\mu_X = \mu_{X^*}$ , this system reduces to an instantiation of the Mandal and Jarzynski device [21] with  $X/X^*$  as bits and the chemical bath as a work reservoir. In this case, the device is driven purely by the input of bits of low “information entropy”. Using an enzyme in this context was proposed in Ref. [23], but without a physical tape. Our setup emphasises that although a notation of 0s and 1s might be used, the Mandal and Jarzynski device is powered by a non-equilibrium supply of physical fuel – an  $X$  or  $X^*$  – just like other machines, consistent with Landauer’s insight that information registers are physical. For general  $\mu_X$  and  $\mu_{X^*}$ , equilibrium states have  $H_{\text{eq}}(A_n) < H_{\text{max}} = \ln 2$ . One cannot, therefore, infer that tape  $A$  is a fuel source from  $H(A_n)$  alone without considering  $\mu_X$  and  $\mu_{X^*}$ .

The presence of  $B$  provides an additional positive contribution to the free energy of the tapes,  $k_B T I(A_n; B_n)$  (Eq. 1). Physically, the enzyme’s decision-making interaction with  $B_n$  determines its response to an incoming  $A_n$ , since  $A_n$  is fixed when  $B_n = \bar{Y}$ . If  $Y$  is correlated with  $X^*$ , then  $X^* + \text{ADP} \rightarrow X + \text{ATP}$  can be favoured over  $X + \text{ATP} \rightarrow X^* + \text{ADP}$ , *allowing extraction of work even if  $\tilde{F}(A_n) - F_{\text{eq}}(A_n) = 0$* . We note that, unlike  $H_{\text{max}} - H(A_n)$ ,  $I(A_n; B_n) \neq 0$  always implies a source of free energy. If there is no initial correlation between  $A_n$  and  $B_n$ , the presence of excess ATP will preferentially convert  $A_n$  to  $X^*$  when  $B_n = Y$ , creating mutual information by expending chemical free energy.

The specificity of DNA origami assembly [38, 39] allows for the construction of a polymer with regularly spaced

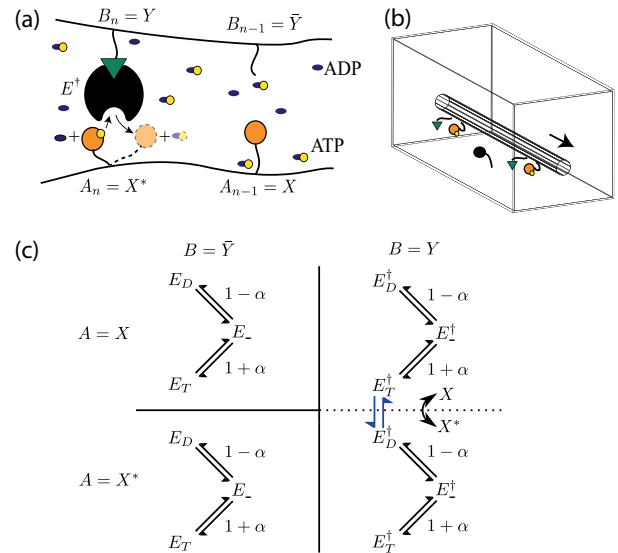


FIG. 1. (a) A system schematic, showing an enzyme interacting with the  $n^{\text{th}}$  pair of sites and catalysing dephosphorylation of the substrate  $X^*$  on tape  $A$  due to the presence of activator  $Y$  on tape  $B$ . Yellow circles correspond to phosphorylation of nucleotides or  $X$ . (b) Illustration of the two tapes, mounted on a single polymer and thereby allowing coordination, being pulled past a tethered enzyme through external manipulation. We propose a DNA origami-based construction (see Appendix A). (c) State space diagram for the model.  $E_A$  and  $E_D$  correspond to ATP- and ADP-bound enzymes, respectively;  $E_-$  to a free enzyme. All unlabelled transitions have rate 1. The blue arrows denote the reaction  $X + \text{ATP} \rightleftharpoons X^* + \text{ADP}$ .

binding sites, to which proteins in different states could be selectively attached. A proposal for instantiating the system, replete with correlations, is given in Appendix A; here we analyse a simple model of device operation. Recall that  $p_0(A_n = X^*) = q$  and that  $A_n, B_n$  are initially independent of  $A_m, B_m$  for  $n \neq m$ . For simplicity we specify initial correlations, through a single parameter  $\psi$ , to be:

$$p_0(B_n = \bar{Y} | A_n = X^*) = p_0(B_n = Y | A_n = X) = \psi, \\ p_0(B_n = Y | A_n = X^*) = p_0(B_n = \bar{Y} | A_n = X) = 1 - \psi.$$

We adjust the chemical load from the bath via  $\alpha \in (-1, 1)$  such that  $[\text{ATP}] = 1 + \alpha$  and  $[\text{ADP}] = 1 - \alpha$  relative to a reference concentration  $C_0$ .

We model the manipulation of the tapes as exposing  $A_n$  to the enzyme for a time  $\tau$ ; we assume that allostery and the binding of  $E$  to  $Y$  are sufficiently strong that the enzyme is active during  $\tau$  if  $Y$  is present, but inactive otherwise. We consider the following reactions: binding/unbinding of nucleotides and  $E$ , and the catalytic inter-conversion of Eq. 2. Enzyme/substrate unbinding is assumed to be sufficiently fast compared to binding that catalysis is instantaneous. For simplicity, we set all rate constants to unity ( $1/C_0$  for bimolecular rate constants), and assume that  $\mu_{\text{ADP}} - \mu_{\text{ATP}} = kT \ln \frac{1-\alpha}{1+\alpha}$ , implying that  $\mu_X = \mu_{X^*}$  given our choice of rate constants

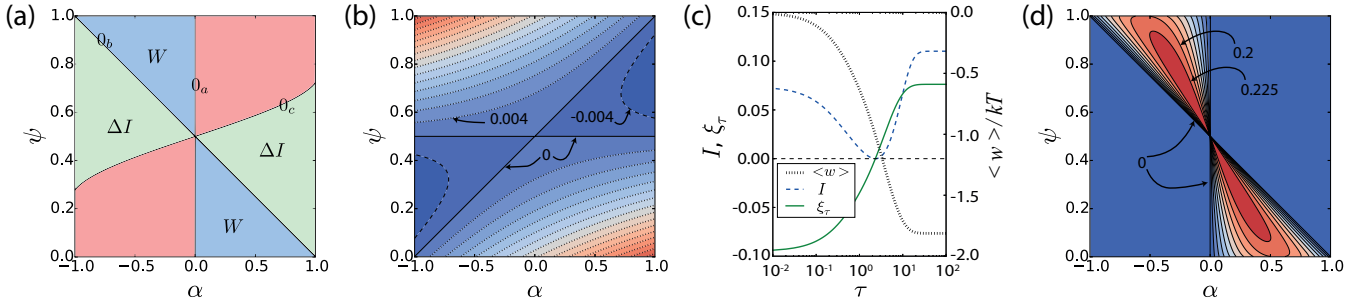


FIG. 2. (a) Regimes of operation for  $q = 0.5$ ,  $\tau \rightarrow \infty$ :  $W$  indicates  $\langle w_{cycle} \rangle > 0$ ,  $\Delta I$  indicates  $\Delta I(A_n; B_n) > 0$ ;  $\langle w_{cycle} \rangle$  and  $\Delta I(A_n; B_n)$  are negative elsewhere. (b) Product of correlations  $\xi_0(A_n, B_n)\xi_\tau(A_n, B_n)$  for  $q = 0.5$ ,  $\tau \rightarrow \infty$ , indicating the possibility of correlation reversal. Negative contours are dashed lines, positive are dotted and zero is solid (contours separated by units of 0.004). (c) Behaviour of  $\langle w_{cycle} \rangle$ ,  $\Delta I(A_n; B_n)$  and correlation  $\xi_\tau(A_n, B_n)$  as a function of  $\tau$  for  $q = 0.5$ ,  $\alpha = -0.99$  and  $\psi = 0.31$ , showing non-monotonicity of information. (d) Efficiency  $\eta$  giving the fraction of initially stored information converted into work. Contours run downwards from 0.225 with a separation of 0.025.

– we relax these assumptions in Appendix C. A central assumption is the large separation of timescales between intended reactions and spontaneous leaks or activator-free catalysis. In practice, these unintended reactions (which can in principle be engineered to be extremely slow) will limit the operation time. The model gives rise to the transition graph shown in Fig. 1 c, which defines a reaction rate matrix  $\mathcal{R}$  that specifies the system evolution via  $p_t = e^{\mathcal{R}t}p_0$ . Since the enzyme relaxes to equilibrium between events, and different pairs of sites are independent, it is sufficient to analyse the evolution of a single pair  $A_n, B_n$ . Full solutions are given in Appendix B.

For  $\tau \rightarrow \infty$ , substrates that are paired with an activator ( $B_n = Y$ ) relax to equilibrium with the bath. The outcome is then determined by the free energy change of reaction,  $\mu_{ADP} + \mu_{X^*} - \mu_{ATP} - \mu_X = kT \ln \frac{1-\alpha}{1+\alpha}$ . If  $\alpha$  is positive, for example, equilibrium with the bath favours an excess of  $X^*$ . The device can only do work on the bath if the substrates encountered by active enzymes are even more likely to be in state  $X^*$  than this excess.

For  $q = 0.5$ , tape  $A$  is initially in the equilibrium determined by  $\mu_X$  and  $\mu_{X^*}$ ,  $\tilde{F}_0(A_n) = F_{eq}(A_n)$ , and hence cannot be used to do work in isolation. Since  $B_n$  does not evolve, from Eq. 1 the only source of free energy is  $I(A_n; B_n)$ . Intuitively,  $E^\dagger$  encounters an excess of  $X^*$  ( $X$ ) if  $\psi < 0.5$  ( $\psi > 0.5$ ). The work done per cycle (the net conversion of  $X^*$  to  $X$  multiplied by  $\mu_{ATP} - \mu_{ADP}$ ) and change in mutual information are calculated in Appendix B. For  $q = 0.5$  and  $\tau \rightarrow \infty$ , there are three regimes of operation, as shown in Fig. 2 a. Using  $\Delta$  as the change of a quantity during  $\tau$ , we see  $\Delta I(A_n; B_n) > 0$  and  $\langle w_{cycle} \rangle < 0$ ;  $\Delta I(A_n; B_n) < 0$  and  $\langle w_{cycle} \rangle > 0$ ; and  $\Delta I(A_n; B_n), \langle w_{cycle} \rangle < 0$ . The device is therefore capable of using information to do work and consuming work to create information, as expected.

The curves that divide the regimes of operation provide significant insight. Along the line identified as  $0_a$  in Fig. 2 a ( $\alpha = 0$ ), no work is performed since there is no chemical load:  $\mu_{ATP} = \mu_{ADP}$ . On  $0_b$  ( $\alpha = 1 - 2\psi$ ), the mutual information drive exactly balances

the chemical load and so there is no net evolution and  $\Delta I(A_n; B_n) = \langle w_{cycle} \rangle/kT = 0$ . The contour  $0_c$ , along which  $\Delta I(A_n; B_n) = 0$ , implies initial alignment between the chemical load and the information drive. As reactions proceed, the correlations between  $A_n$  and  $B_n$  drop and eventually reverse due to the strength of driving. Thus the system generates correlations of the opposite sign that are eventually strong enough to halt the system; this reversal of correlations is shown in Fig. 2 b.

Finite- $\tau$  interaction windows show the reversal of correlations and non-monotonic behaviour of  $I(A_n; B_n)$  (shown in Fig. 2 c for  $\alpha = -0.99$  and  $\psi = 0.31$ , parameters close to the  $0_c$  locus). Indeed, this non-monotonic behaviour is the main effect of finite  $\tau$  (see Appendix C). The reversal of correlations demonstrates the difference between the size of the information reservoir and the chemical bath, and is akin to connecting a charged capacitor and a constant voltage supply to a resistor. Initially, the capacitor and supply drive current in the same direction; eventually, however, the capacitor discharges and then recharges with the opposite polarity.

We plot the fraction of the initial mutual information converted into work,  $\eta = \langle w_{cycle} \rangle/k_B T I(A_n; B_n)$ , in Fig. 2 d. The maximum  $\eta$  is  $\sim 1/4$ . This optimum is midway between  $0_a$  and  $0_b$ , and represents a fundamental trade-off. Near  $0_b$ , the system operates near to equilibrium. Thus the evolution involves negligible dissipation, but also very little actual change during  $\tau$ , so almost none of the initial information is utilised. Near  $0_a$ , the system evolves significantly during  $\tau$ , but does so highly irreversibly (the chemical load is small and thus little work is extracted). Further analysis of efficiency is provided in Appendix B.

For  $q \neq 0.5$ ,  $\tilde{F}_0(A_n) \neq F_{eq}(A_n)$  ( $X$  and  $X^*$  are not in the equilibrium determined by  $\mu_X$  and  $\mu_{X^*}$ ), and tape  $A$  is a source of free energy in and of itself. New regimes of behaviour arise, shown in Fig. 3 a for  $q = 0.7$ , and we observe that information can be used to *enhance* work extraction from a non-equilibrium fuel source. We see all sign permutations of  $\Delta \tilde{F}(A_n)$ ,

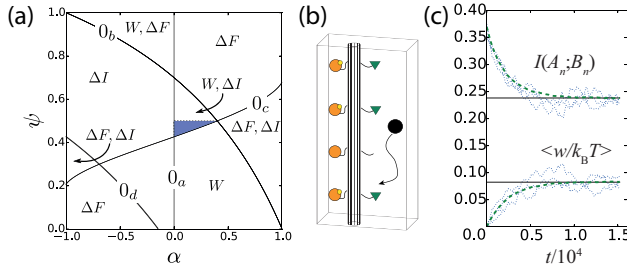


FIG. 3. (a) Regimes of behaviour for  $q = 0.7$ ,  $\tau \rightarrow \infty$ :  $\Delta F$  indicates  $\Delta \tilde{F}(A_n) > 0$ ;  $W$  and  $\Delta I$  are defined equivalently. Highlighted (blue) region has  $\Delta I(A_n; B_n) \geq 0$  and a greater  $\langle w_{\text{cycle}} \rangle$  than for a system with the same  $q, \alpha$ , but with  $I(A_n; B_n) = 0$  initially. (b) A completely autonomous device in which a freely-diffusing enzyme interacts with correlated tapes. (c) Dynamics of the autonomous system, with  $q = 0.5$ ,  $\psi = 0.1$  and  $\alpha = 0.5$ . In addition to the rate constants in Fig. 1c, it is necessary to define a rate at which the enzyme binds to activator  $Y$  ( $k_{\text{bind}} = 0.01$  per activator here) and an unbinding rate ( $k_{\text{off}} = 1$  here). We plot the average work per site  $\langle w \rangle / kT$  and  $I(A_n; B_n)$  obtained from 200 independent Gillespie simulations of 1000 pairs of sites [40] (dashed lines), showing that they converge to the values predicted in the  $\tau \rightarrow \infty$  limit of the externally controlled device (solid lines). Dotted lines show information and work within three individual simulations (see Appendix F for a discussion of subtleties in this comparison).

$\Delta I(A_n; B_n)$  and  $\langle w_{\text{cycle}} \rangle$  except for the second law-violating  $\Delta \tilde{F}(A_n)$ ,  $\Delta I(A_n; B_n)$ ,  $\langle w_{\text{cycle}} \rangle > 0$ . The initial value of  $\tilde{F}(A_n) \neq F_{\text{eq}}(A_n)$  distorts the regimes and introduces a new boundary,  $0_d$ . Line  $0_d$  is analogous to  $0_c$ : along  $0_d$ , the probabilities of  $X^*$  and  $X$  are inverted by machine operation, preserving  $\tilde{F}(A_n) = \tilde{F}_0(A_n)$ .

Given that a region with  $\Delta I(A_n; B_n)$ ,  $\langle w_{\text{cycle}} \rangle > 0$  exists, an imbalanced tape  $A$  can drive the creation of both work and information. Mechanistically, an excess of  $X^*$  can drive ATP production against a chemical load, producing positive work. It can also drive an increase in  $I(A_n; B_n)$  in certain regimes, since the conversion of  $X^* \rightarrow X$  will occur selectively at sites with  $B_n = Y$ .

Mutual information allows for increased work extraction in two ways. The most intuitive is analogous to the  $q = 0.5$  case:  $I(A_n; B_n)$  is consumed to drive catalysis against the bath's chemical load. More surprisingly, in the highlighted region of Fig. 3a,  $\Delta I(A_n; B_n) \geq 0$  yet  $\langle w_{\text{cycle}} \rangle$  is increased relative to an otherwise equivalent system that lacks pre-existing  $I(A_n; B_n)$ . Here, correlations initially support the drive from  $\tilde{F}(A_n) \neq F_{\text{eq}}(A_n)$  to do work against the bath, but eventually reverse and oppose further reactions. The need to reverse the initial correlations allows more production of ATP before the reaction halts, enhancing  $\langle w_{\text{cycle}} \rangle$  despite  $\Delta I(A_n; B_n) \geq 0$ .

Each trajectory  $z(t) = (e(t), a_n(t), b_n(t))$ , with  $e(t)$ ,  $a_n(t)$  and  $b_n(t)$  representing the states of  $E$ ,  $A_n$  and  $B_n$  over time, has a stochastic entropy  $\sigma[z(t), p_t(z)]$ , a

functional of  $z(t)$  and the probability of the system occupying state  $z$  at time  $t$ ,  $p_t(z)$  [41–43]. With  $b_n(t)$  constant, the fluctuation relation  $\langle e^{-\sigma[z(t), p_t(z)]/k_B} \rangle = 1$  implies  $\langle e^{-\bar{\sigma}[e_n(t), a_n(t), p_t(e, a_n)]/k_B + \Delta i_{0,\tau}(b_n; e, a_n)} \rangle = 1$ , where  $\bar{\sigma}$  is the stochastic entropy generated by the  $(E, A_n)$  subsystem and  $i(b_n; e, a_n) = \ln(p(b_n, e, a_n)/p(b_n)p(e, a_n))$  is a pointwise mutual information [17]. Together with the related inequality  $\langle \bar{\sigma}[e(t), a_n(t), p_t(e, a_n)] \rangle \geq \Delta I_{0,\tau}(B_n; E, A_n)$ , the fluctuation theorem predicts that consumption of mutual information allows for entropy reduction elsewhere – manifest here as  $\Delta F(A_n) > 0$  or  $\langle w_{\text{cycle}} \rangle > 0$ . Unusually, in our model the fluctuation theorem is explicitly verifiable via summation over trajectories (see Appendix D).

Our concrete construction of the device in Fig. 1a,b emphasises that the information register must physically couple to the device, a fact often ignored. If the tapes are pulled at a finite rate, irreversible work will be done on the protein-protein interactions. If this dissipation is to be minimised through slow manipulation of the tapes, it sets requirements on the intrinsic stability of the phosphorylation states of  $X$ . Additional subtleties also arise when unidirectional motion is imposed externally [44], as outlined in Appendix E. These problems can be eliminated if the device functions in a truly autonomous way, with no external manipulation after initiation. To this end we propose a modified system analogous to Fig. 1, but with an enzyme that is free to diffuse between sites rather than requiring the tape to be pulled (Fig. 3b). The dynamics of such a system are more complex, with the enzyme able to repeatedly return to the same pair of sites, but the principle that correlation of the tapes allows selective interaction with either  $X$  or  $X^*$  remains. Indeed, regardless of the dynamical details, the systems are closely related in the limit of long times (large interaction window  $\tau$  for the non-autonomous system). In both cases, the enzyme allows those substrates paired with  $Y$  to relax to equilibrium with the bath, and thus the limiting distribution is the same for a given set of  $\alpha$ ,  $\psi$  and  $q$ . Thus, as shown in Fig. 3c, the long-time average behaviour of the autonomous system is equivalent to the  $\tau \rightarrow \infty$  limit of the non-autonomous system, and all previously reported behaviour is replicated. The limit also holds if multiple enzymes are present, allowing faster operation.

We have introduced devices for interconverting chemical work and mutual information within the environment that are based on concrete biophysical processes, including an autonomous example. Our devices emphasize the physical nature of information and its role as a thermodynamic resource. In principle, the chemical free energy generated could be used to power a molecular motor, generating mechanical work. The devices lack memory, in the sense that the information utilised is the correlation between degrees of freedom that are encountered simultaneously. Designing systems that can harness time correlations within a signal is the subject of future work.

- 
- [1] C. E. Shannon and W. Weaver, *The mathematical theory of communication* (University of Illinois Press, 1949).
- [2] C. C. Govern and P. R. ten Wolde, Phys. Rev. Lett. **113**, 258102 (2014).
- [3] A. C. Barato, D. Hartich, and U. Seifert, New. J. Phys. **16**, 103024 (2014).
- [4] T. E. Ouldridge, C. C. Govern, and P. R. ten Wolde, arXiv:1503.00909.
- [5] R. Cheong, A. Rhee, C. J. Wang, I. Nemenman, and A. Levchenko, Science **334**, 354 (2011).
- [6] W. de Ronde, F. Tostevin, and P. R. ten Wolde, Phys. Rev. Lett. **107**, 048101 (2011).
- [7] P. Sartori, L. Granger, C. F. Lee, and J. M. Horowitz, PLoS Comput Biol **10**, e1003974 (2014).
- [8] S. Ito and T. Sagawa, Nat. Comm. **6**, 7498 (2015).
- [9] G. Micali and R. G. Endres, Curr. Opin. Microbiol. **30**, 8 (2016).
- [10] N. B. Becker, A. Mugler, and P. R. ten Wolde, Phys. Rev. Lett. **115**, 258103 (2015).
- [11] W. Bialek, arXiv:1512.08954 (2015).
- [12] R. Landauer, IBM J. Res. Dev. **5**, 183 (1961).
- [13] C. H. Bennett, Int. J. Theor. Phys. **21**, 905 (1982).
- [14] T. Sagawa and M. Ueda, Phys. Rev. Lett. **102**, 250602 (2009).
- [15] M. Bauer, D. Abreu, and U. Seifert, J. Phys. A-Math. Theor. **45**, 162001 (2012).
- [16] S. Still, D. A. Sivak, A. J. Bell, and G. E. Crooks, Phys. Rev. Lett. **109**, 120604 (2012).
- [17] T. Sagawa and M. Ueda, Phys. Rev. Lett. **109**, 180602 (2012).
- [18] J. M. Horowitz and M. Esposito, Phys. Rev. X **4**, 031015 (2014).
- [19] A. C. Barato and U. Seifert, Phys. Rev. Lett. **112**, 090601 (2014).
- [20] J. M. R. Parrondo, J. M. Horowitz, and T. Sagawa, Nat. Phys. **11**, 131 (2015).
- [21] D. Mandal and C. Jarzynski, Proc. Nat. Acad. Sci. USA **109**, 11641 (2012).
- [22] D. Mandal, H. T. Quan, and C. Jarzynski, Phys. Rev. Lett. **111**, 030602 (2013).
- [23] Y. Cao, Z. Gong, and H. T. Quan, Phys. Rev. E **91**, 062117 (2015).
- [24] P. N. Fahn, Found. Phys. **26**, 71 (1996).
- [25] J. M. Horowitz, T. Sagawa, and J. M. R. Parrondo, Phys. Rev. Lett. **111**, 010602 (2013).
- [26] M. Esposito and C. Van Den Broeck, Europhys. Lett. **95**, 40004 (2011).
- [27] A. C. Barato and U. Seifert, Europhys. Lett. **101**, 60001 (2013).
- [28] Z. Lu and D. M. M. Jarzynski, Phys. T **67**, 60 (2014).
- [29] A. B. Boyd, D. Mandal, and J. P. Crutchfield, New J. Phys. **18**, 023049 (2016).
- [30] A. Chapman and A. Miyake, Phys. Rev. E **92**, 062125 (2015).
- [31] S. Toyabe, T. Sagawa, M. Ueda, E. Muneyuki, and M. Sano, Nat. Phys. **6**, 988 (2010).
- [32] M. D. Vidrighin, O. Dahlsten, M. Barbieri, M. S. Kim, V. Vedral, and I. A. Walmsley, Phys. Rev. Lett. **116**, 050401 (2016).
- [33] R. Landauer, Phys. Today **44**, 23 (1991).
- [34] E. Zeqiraj, B. M. Filippi, M. Deak, D. R. Alessi, and D. M. F. van Aalten, Science **326**, 1707 (2009).
- [35] S. W. Cowan-Jacob, W. Jahnke, and S. Knapp, Future Med. Chem. **6**, 541 (2014).
- [36] Y. Qiao, H. Molina, A. Pandey, J. Zhang, and P. A. Cole, Science **311**, 1293 (2006).
- [37] A. V. Karginov, F. Ding, P. Kota, N. V. Dokholyan, and K. M. Hahn, Nat. Biotechnol. **28**, 743 (2010).
- [38] P. W. K. Rothemund, Nature **440**, 297 (2006).
- [39] S. M. Douglas, H. Dietz, T. Liedl, B. Höglberg, F. Graf, and W. M. Shih, Nature **459**, 414 (2009).
- [40] D. T. Gillespie, J. Phys. Chem. **81**, 2340 (1977).
- [41] G. E. Crooks, Phys. Rev. E **60**, 2721 (1999).
- [42] U. Seifert, Eur. Phys. J. E **34**, 26 (2011).
- [43] U. Seifert, Rep. Prog. Phys. **75**, 126001 (2012).
- [44] B. B. Machta, Phys. Rev. Lett. **115**, 260603 (2015).

## Appendix A: Construction and setup of the device

A proposal for the construction of correlated tapes is illustrated in Fig. 4. By mixing single-stranded DNA species with well-designed sequences, a long scaffold strand could be folded into a bundle of helices with “sticky ends” that are available for subsequent bonding [38, 39]. Using the sticky ends, these bundles could then be assembled into long polymers, with the persistence length of these structures tuned through the bundle geometry. Importantly, the polymers consist of repeated units which themselves contain multiple distinct strands, each in a precise location. We propose to manipulate one of these strands in two ways.

- First, we extend the ends of the strand so that when incorporated into the structure, it possesses two dangling recognition domains  $P_1$  and  $Q_1$ .
- We introduce a second copy of the strand with distinct recognition domains,  $P_2$  and  $Q_2$ .

When the polymer is assembled, it will consist of multiple evenly spaced pairs of recognition domains sites, which will randomly be either  $(P_1, Q_1)$  or  $(P_2, Q_2)$ ; the proportion can be tuned by varying the initial strand concentration. Such a configuration is illustrated as the third step in Fig. 4.

The substrate protein  $X$  could be conjugated with DNA strands via a variety of methods. We propose preparing two separate systems of  $X$ -conjugated DNA, one with  $X$  conjugated to a strand complementary to  $P_1$ ,  $\bar{P}_1$ , and one with  $X$  conjugated to a strand complementary to  $P_2$ ,  $\bar{P}_2$ . The first system would be exposed to kinases and an ATP dominated bath to drive it to the  $X^*$ -dominated state, the second system to phosphatases in a phosphate-depleted bath to drive it to the  $X$  state. The strands would then be separated from the buffers (perhaps by anchoring them to surface-immobilized origami and washing out the buffer, before breaking the anchorage by displacement). Finally, they are mixed with the

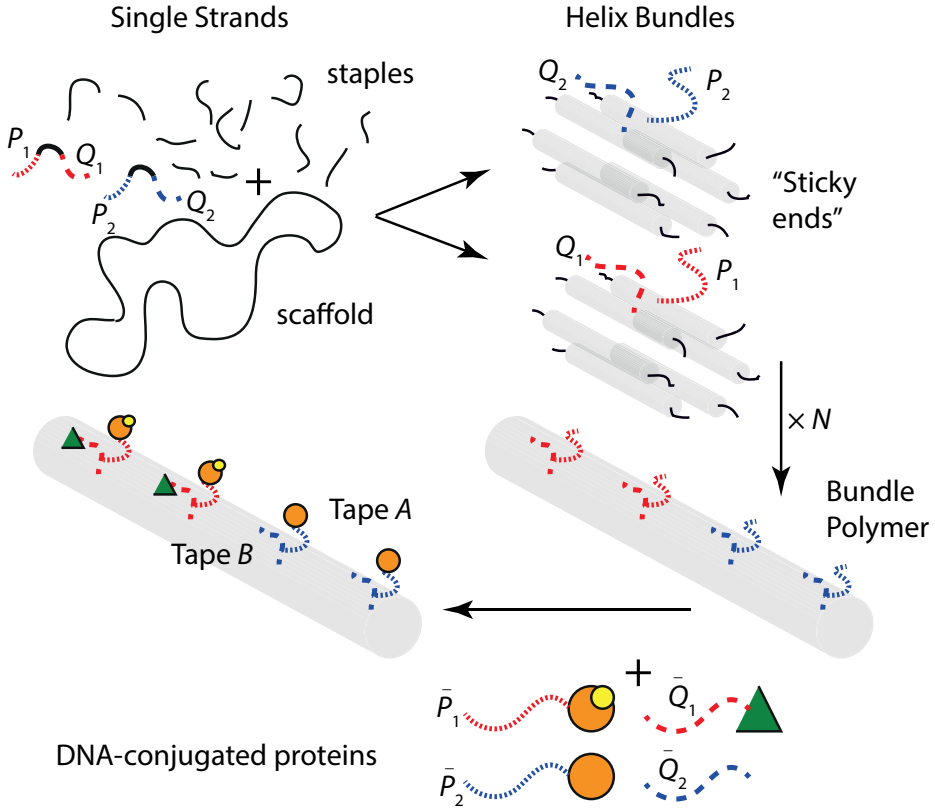


FIG. 4. Schematic diagram showing the construction of a correlated and coordinated pair of tapes using DNA origami. Firstly, long single-stranded DNA scaffolds are assembled into short helix bundles (the small grey tubes are a single bundle) by short staples with carefully selected sequences [38, 39]. Each bundle incorporates one of two staple types that present distinct single-stranded recognition domains. Bundles then assemble into long polymers (large grey tube) through binding of complementary “sticky ends”. Finally, DNA conjugated proteins are mixed with the polymer to create fully-formed tapes. Biasing the state of the conjugated proteins, as indicated, leads to correlations in the final polymer.

wires to generate a random sequence of  $X$  and  $X^*$  along the wire.

We also propose to conjugate  $Y$  with strands of type  $\bar{Q}_1$  and  $\bar{Q}_2$ . In the main text we suggest an activator  $Y$  that consists of two molecules, STRAD and MO25 – in this case, the two molecules can be co-localized by conjugation with either end of a strand. We also prepare solutions of  $\bar{Q}_1$  and  $\bar{Q}_2$  strands with no conjugated  $Y$  molecules. The solutions can then be simultaneously mixed with the wires, and  $Q$  sites on the wire will be occupied in a manner that depends on the relative frequency of conjugated and un-conjugated  $\bar{Q}_1$  and  $\bar{Q}_2$ , and the excess washed off.

The result of this process would be a single polymer wire containing two parallel tracks (or tapes), one of which contains  $X/X^*$  and the other  $Y/\bar{Y}$ . If the majority of  $\bar{Q}_1$  strands mixed with the wires were conjugated to  $Y$ , but the majority of  $\bar{Q}_2$  strands were not, the presence of  $X^*$  on a site will be correlated with the presence of  $Y$ . Fig. 4 illustrates this outcome for the case in which this correlation is perfect; alternative choices lead to weaker or reversed correlations.

The enzyme could be tethered to a surface-immobilised origami, and the tapes pulled past it in the appropriate bath of nucleotides to operate the device. In the autonomous case, the enzyme and the wire would simply need to be added to solution. Provided the recognition sites that link  $Y$  and  $X$  to the wire are sufficiently long to allow simultaneous interaction with  $E$ , but also short enough to prevent cross-talk between sites, the model provided in the text provides an approximate description of device operation. Choosing a relatively stiff polymer wire construction would limit cross-talk.

## Appendix B: Solution of the model

We now discuss the solution of the model presented in Fig. 1c of the main text. The enzyme is allowed to reach equilibrium with the ATP/ADP bath in between encountering sites  $n$  and  $n + 1$ ; therefore it is sufficient to analyse each doublet  $(A_n, B_n)$  independently. Since, during the interaction window, the state of site  $B_n$  implies the activation state of the enzyme, our state space is

12-dimensional (as per Fig. 1c of the main text) and characterised by the time-dependent probability  $p_t(e, a_n, b_n)$ , where  $e$  is the state of  $E$ ,  $a_n$  is the state of the substrate  $A_n$  and  $b_n$  is the state of the activator  $B_n$ . Here the possible states of  $E$  are  $E_-$  (no nucleotide bound),  $E_T$  (ATP bound) and  $E_D$  (ADP bound), plus activated counterparts, the possible states of  $A_n$  are  $X$  and  $X^*$  and the possible states of  $B_n$  are  $Y$  and  $\bar{Y}$ . Working with the vector  $p_t(e, a_n, b_n)$  defined as

$$p_t(e, a_n, b_n) = \begin{pmatrix} p_t(E = E_D, A_n = X, B_n = \bar{Y}) \\ p_t(E = E_-, A_n = X, B_n = \bar{Y}) \\ p_t(E = E_T, A_n = X, B_n = \bar{Y}) \\ p_t(E = E_D, A_n = X^*, B_n = \bar{Y}) \\ p_t(E = E_-, A_n = X^*, B_n = \bar{Y}) \\ p_t(E = E_T, A_n = X^*, B_n = \bar{Y}) \\ p_t(E = E_D^\dagger, A_n = X, B_n = Y) \\ p_t(E = E_-^\dagger, A_n = X, B_n = Y) \\ p_t(E = E_T^\dagger, A_n = X, B_n = Y) \\ p_t(E = E_D^\dagger, A_n = X^*, B_n = Y) \\ p_t(E = E_-^\dagger, A_n = X^*, B_n = Y) \\ p_t(E = E_T^\dagger, A_n = X^*, B_n = Y) \end{pmatrix}, \quad (B1)$$

the evolution of the system during the window  $t = 0 \rightarrow \tau$  is given by  $p_t(e, a_n, b_n) = e^{\mathcal{R}t} p_0(e, a_n, b_n)$ , where  $\mathcal{R}$  is the transition rate matrix

$$\mathcal{R} = \begin{pmatrix} \mathcal{R}_{\bar{Y}} & 0 \\ 0 & \mathcal{R}_Y \end{pmatrix}. \quad (B2)$$

Here,

$$\mathcal{R}_{\bar{Y}} = \begin{pmatrix} -1 & 1 - \alpha & 0 & 0 & 0 & 0 \\ 1 & -2 & 1 & 0 & 0 & 0 \\ 0 & 1 + \alpha & -1 & 0 & 0 & 0 \\ 0 & 0 & 0 & -1 & 1 - \alpha & 0 \\ 0 & 0 & 0 & 1 & -2 & 1 \\ 0 & 0 & 0 & 0 & 1 + \alpha & -1 \end{pmatrix}, \quad (B3)$$

and

$$\mathcal{R}_Y = \begin{pmatrix} -1 & 1 - \alpha & 0 & 0 & 0 & 0 \\ 1 & -2 & 1 & 0 & 0 & 0 \\ 0 & 1 + \alpha & -2 & 1 & 0 & 0 \\ 0 & 0 & 1 & -2 & 1 - \alpha & 0 \\ 0 & 0 & 0 & 1 & -2 & 1 \\ 0 & 0 & 0 & 0 & 1 + \alpha & -1 \end{pmatrix}. \quad (B4)$$

The initial condition is

$$p_0(e, a_n, b_n) = \begin{pmatrix} \mathbb{I}_3(1 - \psi)(1 - q) \\ \mathbb{I}_3\psi q \\ \mathbb{I}_3\psi(1 - q) \\ \mathbb{I}_3(1 - \psi)q \end{pmatrix} \begin{pmatrix} \frac{1 - \alpha}{3} \\ \frac{1}{3} \\ \frac{1 + \alpha}{3} \end{pmatrix}. \quad (B5)$$

In the period after  $\tau$ ,  $A_n$  and  $B_n$  are fixed and  $E$  relaxes back to its equilibrium distribution according to

$$p_{t+\tau}(e) = e^{\mathcal{R}_E t} p_\tau(e), \quad (B6)$$

with  $\mathcal{R}_E$  given by

$$\mathcal{R}_E = \begin{pmatrix} -1 & 1 - \alpha & 0 \\ 1 & -2 & 1 \\ 0 & 1 + \alpha & -1 \end{pmatrix}, \quad (B7)$$

and  $p_t(e) = (p_t(E = E_D), p_t(E = E_-), p_t(E = E_T))^T$ . In the main text we rely on the fact that this relaxation reaches steady state to treat each pair of sites  $n$  independently, but the details of the dynamics are not that important.

The full behaviour can be solved straightforwardly by identifying the eigenvalues and eigenvectors of  $\mathcal{R}$ , but the most important results are

$$\begin{aligned} p_\tau(A_n = X, B_n = Y) &= \\ p_0(B_n = Y) \left( \frac{1 - \alpha}{2} + f(\tau)(p_0(A_n = X | B_n = Y) - \frac{1 - \alpha}{2}) \right), \\ p_\tau(A_n = X^*, B_n = Y) &= \\ p_0(B_n = Y) \left( \frac{1 + \alpha}{2} + f(\tau)(p_0(A_n = X^* | B_n = Y) - \frac{1 + \alpha}{2}) \right), \end{aligned} \quad (B8)$$

along with the trivial

$$p_\tau(A_n = X, B_n = \bar{Y}) = p_0(A_n = X, B_n = \bar{Y}) = (1 - q)(1 - \psi),$$

$$p_\tau(A_n = X^*, B_n = \bar{Y}) = p_0(A_n = X^*, B_n = \bar{Y}) = q\psi. \quad (B9)$$

Here,  $p_0(B_n = Y) = q(1 - \psi) + \psi(1 - q)$ ,  $p_0(A_n = X | B_n = Y) = 1 - p_0(A_n = X^* | B_n = Y) = \psi(1 - q)/(q(1 - \psi) + \psi(1 - q))$ . Finally,

$$f(\tau) = \frac{1}{9} e^{-2\tau} \left( 1 + 8 \cosh(\sqrt{3}\tau) + 4\sqrt{3} \sinh(\sqrt{3}\tau) \right) \quad (B10)$$

is a function of  $\tau$  only that is unity at  $\tau = 0$  and tends monotonically to zero as  $\tau \rightarrow \infty$ . The quantities  $\Delta I(A_n, B_n)$ ,  $\Delta \tilde{F}(A_n)$ ,  $\Delta \tilde{F}(A_n, B_n)$  and  $\langle w_{\text{cycle}} \rangle$ , as plotted in Fig. 5, all follow directly from the results above. Specifically, the work done on the chemical bath per cycle is given by the net number of  $X^*$  molecules converted into  $X$  multiplied by  $\mu_{\text{ATP}} - \mu_{\text{ADP}}$ ,

$$\langle w_{\text{cycle}} \rangle = kT \ln \left( \frac{1 + \alpha}{1 - \alpha} \right) (q - p_\tau(A_n = X^*)). \quad (B11)$$

The mutual information  $I(A_n; B_n)$  follows directly in terms of the marginal and joint probabilities, and

$$\tilde{F}(A_n) = -kT H(A_n) = kT \sum_{a_n} p(a_n) \ln p(a_n), \quad (B12)$$

in this simple case in which  $\mu_X = \mu_{X^*}$ . Since  $B$  does not evolve,  $\Delta \tilde{F}(A_n, B_n) = \Delta \tilde{F}(A_n) + k_B T I(A_n; B_n)$ .

## 1. Work and Information change for $q = 0.5, \tau \rightarrow \infty$

In Fig. 5 we plot  $\langle w_{\text{cycle}} \rangle$  and  $\Delta I(A_n; B_n)$  for the first case considered in the main text,  $q = 0.5, \tau \rightarrow \infty$ . These

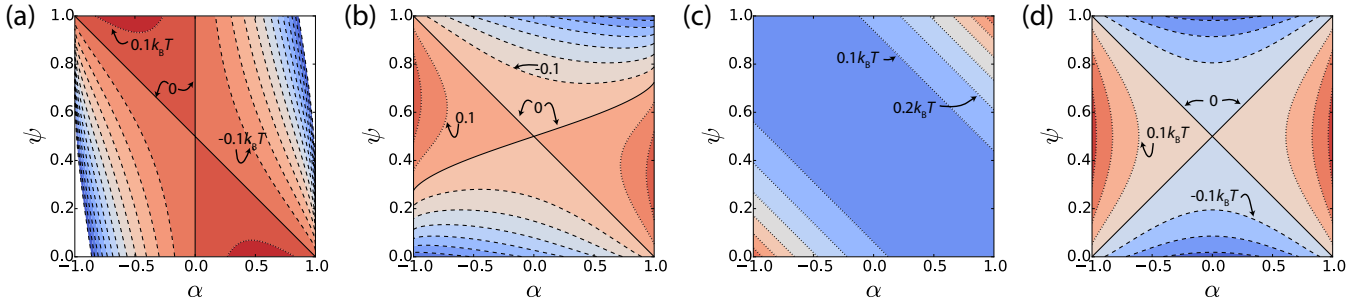


FIG. 5. Behaviour for  $q = 0.5$ ,  $\tau \rightarrow \infty$ . (a) Work extracted  $\langle w_{\text{cycle}} \rangle$ , with contours running downwards from  $0.1kT$  in units of  $0.1kT$ . (c) Information change  $\Delta I(A_n; B_n)$ , with contours running downwards from  $0.2$  in units of  $0.1$ . (c) Free-energy change in tape  $A$ ,  $\Delta \tilde{F}(A_n)$ , with contours running upwards from  $0.1k_B T$  in units of  $0.1k_B T$ . (d) Change in the combined free energy of both tapes  $\Delta \tilde{F}(A_n, B_n)$ , with contours running downwards from  $0.3k_B T$  in units of  $0.1k_B T$ . In all cases, solid contours indicate  $0$ , dotted contours are positive values and dashed contours are negative.

contour plots imply the regimes indicated in Fig. 2,a of the main text. We also include  $\Delta \tilde{F}(A_n)$ , which is always positive since  $q = 0.5$  represents equilibrium between  $X$  and  $X^*$ ,  $\tilde{F}(A_n) = F_{\text{eq}}(A_n)$ . For completeness, we plot  $\Delta \tilde{F}(A_n, B_n) = \Delta \tilde{F}(A_n) + k_B T \Delta I(A_n; B_n)$ .

## 2. Efficiency

There are many possible definitions of the efficiency of this device. From the perspective of work and information only, we could consider

$$\eta_1^I = \begin{cases} -\langle w_{\text{cycle}} \rangle / kT \Delta I(A_n; B_n) & \text{if } \langle w_{\text{cycle}} \rangle > 0, \\ -kT \Delta I(A_n; B_n) / \langle w_{\text{cycle}} \rangle & \text{if } \Delta I(A_n; B_n) > 0, \\ 0 & \text{otherwise,} \end{cases} \quad (\text{B13})$$

which is the fraction of the information reduction converted into work, or the fraction of chemical work converted into stored information, respectively. We could also consider the fraction of initially available information that is converted into work,

$$\eta_2^I = \begin{cases} \langle w_{\text{cycle}} \rangle / kT I_0(A_n; B_n) & \text{if } \langle w_{\text{cycle}} \rangle > 0, \\ 0 & \text{otherwise.} \end{cases} \quad (\text{B14})$$

This approach treats any information remaining between  $A_n$  and  $B_n$  as waste. The efficiency  $\eta_2^I$  is the quantity discussed under the name  $\eta$  in the main text. Both  $\eta_1^I$  and  $\eta_2^I$  also treat free energy stored in  $A_n$  by the device at the end of the cycle,  $\tilde{F}_\tau(A_n)$ , as waste. We can define similar efficiencies  $\eta_1^F$  and  $\eta_2^F$  in which  $\tilde{F}(A_n, B_n)$  replaces  $I(A_n; B_n)$  in Eqs. B13, to treat all free energy within the tapes on an equal footing.

We plot  $\eta_1^I$  and  $\eta_1^F$  for  $q = 0.5$  in Fig. 6 (in this case,  $\eta_2^F = \eta_2^I$ , plotted in Fig. 2d of the main text).  $\eta_1^I \rightarrow 1$  on the null line  $0_b$ , when the system deviates only a small amount from equilibrium. However, in this case a vanishingly small amount of the information is used, as illustrated by the plot of  $\eta_2^I$  in the main text. As is

evident from Fig. 6,  $\eta_1^F$  is similar to but larger than  $\eta_1^I$  due to the free energy stored in  $A$  not being counted as waste.

## Appendix C: Adjusting input parameters

### 1. Finite $\tau$

We plot  $\langle w_{\text{cycle}} \rangle$ ,  $\Delta I(A_n; B_n)$ ,  $\Delta \tilde{F}(A_n)$  and  $\tilde{F}(A_n, B_n)$  for finite  $\tau = 1$  and  $q = 0.5$  in Fig. 7. The results are similar to  $\tau \rightarrow \infty$  (Fig. 5). Indeed, the lines  $0_a$  and  $0_b$  are unchanged, as expected. The most notable difference is that, since the reaction during  $\tau$  no longer reaches equilibrium, the initial conditions required to lie on the curve  $0_c$  change. Thus  $I(A_n; B_n)$  is non-monotonic in  $\tau$  in some regions of  $\alpha - \psi$  space, as illustrated in Fig. 2c of the main text. In its region of non-monotonicity,  $I(A_n; B_n)$  is initially drained and then restored as the correlations first support and then oppose the thermodynamic drive of the ATP/ADP bath.

### 2. $q \neq 0.5$

In Fig. 8, we plot  $\langle w_{\text{cycle}} \rangle$  and  $\Delta I(A_n; B_n)$  for  $q = 0.7$  and  $\tau \rightarrow \infty$ ; the same values used to produce Fig. 3a of the main text. We also include  $\Delta \tilde{F}(A_n)$  and  $\Delta \tilde{F}(A_n, B_n)$ . Previously, for  $q = 0.5$ , the initial tape  $A$  was in equilibrium with  $\tilde{F}(A_n) = F_{\text{eq}}(A_n)$  and so only positive values of  $\Delta \tilde{F}(A_n)$  were possible (Fig. 5). For  $q \neq 0.5$ ,  $\Delta \tilde{F}(A_n)$  is negative between  $0_b$  and  $0_d$ , introducing the new regimes of behaviour illustrated in Fig. 3a of the main text.

The null line  $0_b$  is now given by  $2\psi(1-q) = (1-\alpha)((1-q)\psi + q(1-\psi))$ , and positive work occupies a larger region for  $\alpha > 0$  (high [ATP]/[ADP]) than  $\alpha < 0$  since  $q > 0.5$  provides an excess of  $X^*$  that tends to convert ADP into ATP. The line  $0_c$  is shifted; a non-equilibrium tape  $A$  can generate  $I(A_n; B_n)$  even when a device is fed with

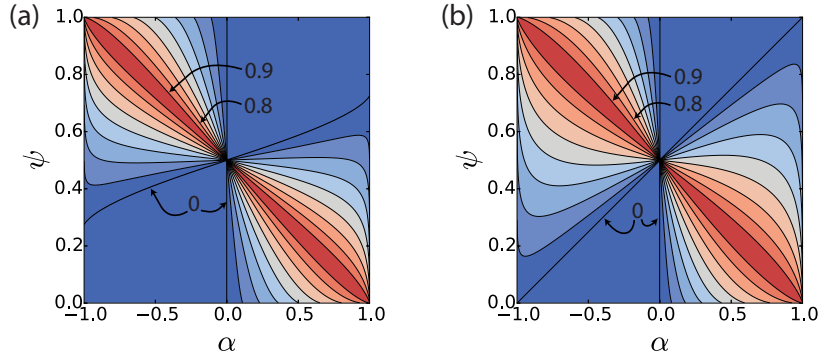


FIG. 6. Efficiencies (a)  $\eta_1^I$  and (b)  $\eta_1^F$  for  $q = 0.5$  and  $\tau \rightarrow \infty$ . The quantity  $\eta_1^I$  represents the fraction of the information reduction converted into work, or the fraction of chemical work converted into stored information;  $\eta_1^F$  is an equivalent quantity in which the entire free energy of the tapes  $F(A_n, B_n)$  is taken into account instead of just  $I(A_n; B_n)$ . In both cases, efficiency is high near the null line  $0_b$  where the system is weakly driven and functions close to equilibrium.

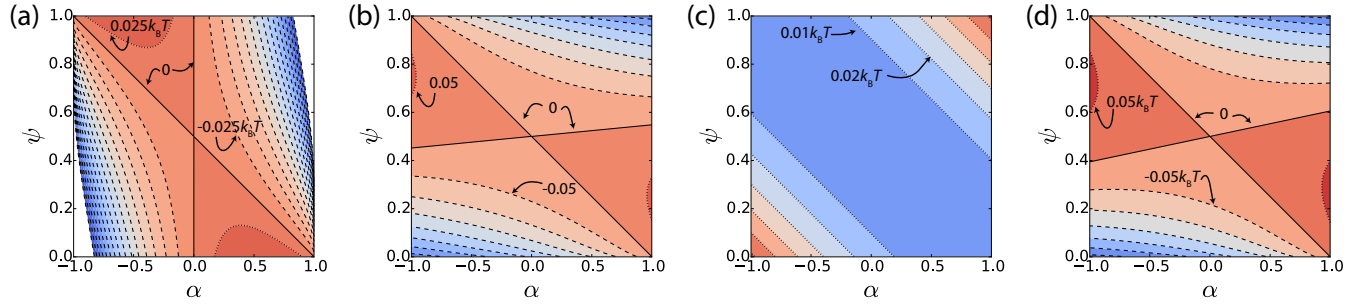


FIG. 7. Behaviour for  $q = 0.5$ ,  $\tau = 1$ , to be compared with Fig. 5. (a) Work extracted  $\langle w_{\text{cycle}} \rangle$ , with contours running downwards from  $0.025k_BT$  in units of  $0.025k_BT$ . (b) Information change  $\Delta I(A_n; B_n)$ , with contours running downwards from  $0.05$  in units of  $0.05$ . (c) Free-energy change in tape  $A$ ,  $\Delta \tilde{F}(A_n)$ , with contours running upwards from  $0.01k_BT$  in units of  $0.01k_BT$ . (d) Change in the combined free energy of both tapes  $\Delta \tilde{F}(A_n, B_n)$ , with contours running downwards from  $0.05k_BT$  in units of  $0.05k_BT$ . In all cases, solid contours indicate 0, dotted contours are positive values and dashed contours are negative.

no information ( $\psi = 0.5$ ) and no imbalance of ATP and ADP ( $\alpha = 0$ ).

### 3. Varying the rates

Instead of setting the majority of rates to be equal, we could consider allowing variability. Retaining the simplification that binding and unbinding of ATP and ADP is independent of whether the enzyme is active or not gives the following set of rate constants:

$$E_- \xrightleftharpoons[k_{-1}^D]{k_1^D(1-\alpha)} E_D, \quad E_- \xrightleftharpoons[k_{-1}^T]{k_1^T(1+\alpha)} E_T, \quad (C1)$$

$$E_D^\dagger + X^* \xrightleftharpoons[k_{-2}]{k_2} E_T^\dagger + X.$$

Additionally, we set  $k_1^T = k_1^D$ , which corresponds to assuming the difference between ATP and ADP binding strength is manifest in the off-rate. Finally, although it does not affect the dynamics, it is necessary to identify an intrinsic free-energy change upon interconversion of

ATP and ADP (which could, in principle, be set by adjusting the concentration of inorganic phosphate in the bath). The free energy change on converting ATP into ADP is given by  $\mu_{\text{ADP}} - \mu_{\text{ATP}} = k_B T \ln \frac{1-\alpha}{1+\alpha} - \Delta F_{\text{D} \rightarrow \text{T}}^0$ ; in the main text  $\Delta F_{\text{D} \rightarrow \text{T}}^0$  was set to zero. This implies an intrinsic free energy difference between  $X^*$  and  $X$  of

$$\Delta F_{X^* \rightarrow X}^0 = \mu_X - \mu_{X^*} = -\Delta F_{\text{D} \rightarrow \text{T}}^0 - k_B T \ln \left( \frac{k_2 k_{-1}^T}{k_{-2} k_{-1}^D} \right), \quad (C2)$$

which was zero under the assumptions of the main text. As a result, unlike the main text and Section B, the free energy of tape  $A$ ,  $\tilde{F}(A_n)$ , is no longer specified purely by its entropy, but contains a contribution from the relative stabilities of  $X$  and  $X^*$ :

$$\tilde{F}(A_n) - \tilde{F}_{\text{eq}}(A_n) = (p(A_n = X^*) - p_{\text{eq}}(A_n = X^*)) (\mu_{X^*} - \mu_X) - k_B T H(A_n). \quad (C3)$$

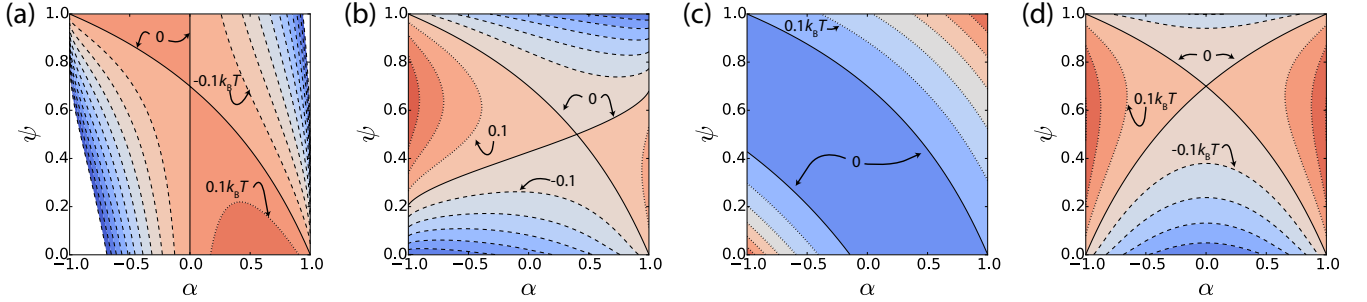


FIG. 8. Behaviour for  $q = 0.7$ ,  $\tau \rightarrow \infty$ , to be compared with Fig. 5. (a) Work extracted  $\langle w_{\text{cycle}} \rangle$ , with contours running downwards from  $0.1k_B T$  in units of  $0.1k_B T$ . (b) Information change  $\Delta I(A_n; B_n)$ , with contours running downwards from  $0.3$  in units of  $0.1$ . (c) Free-energy change in tape  $A$ ,  $\Delta \tilde{F}(A_n)$ , with contours running upwards from  $0k_B T$  in units of  $0.1k_B T$ . (d) Change in the combined free energy of both tapes  $\Delta \tilde{F}(A_n, B_n)$ , with contours running downwards from  $0.2k_B T$  in units of  $0.1k_B T$ . In all cases, solid contours indicate  $0$ , dotted contours are positive values and dashed contours are negative. Note the distortions of the null lines compared to Fig. 5, and the appearance of two contours along which  $\Delta \tilde{F}(A_n) = 0$ , enclosing a region of negative  $\Delta \tilde{F}(A_n)$ .

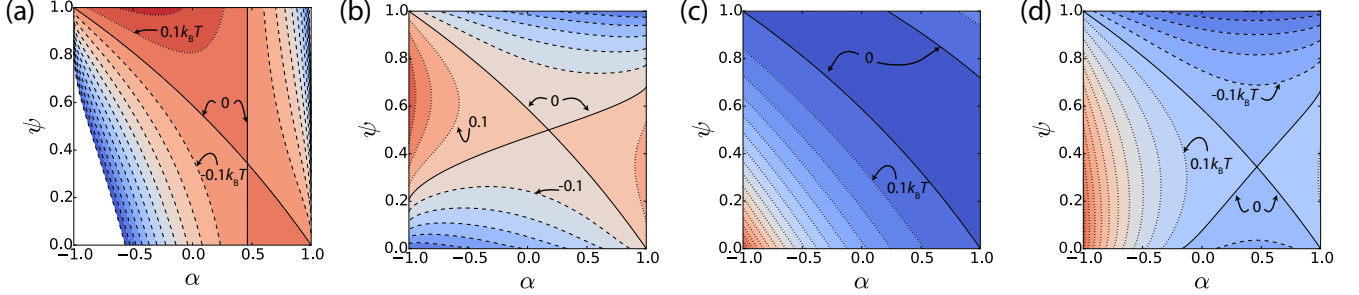


FIG. 9. Behaviour for  $q = 0.7$ ,  $\tau \rightarrow \infty$ , and varied rates. Specifically,  $k_1^T = k_1^D = 1$ ,  $k_{-1}^T = 1.4$ ,  $k_{-1}^D = 0.8$ ,  $k_2 = 0.7$  and  $k_{-2} = 2$  in reduced units. Additionally, we take  $\Delta F_{\text{D} \rightarrow \text{T}}^0 = -1$ . (a) Work extracted  $\langle w_{\text{cycle}} \rangle$ , with contours running downwards from  $0.2k_B T$  in units of  $0.1k_B T$ . (c) Information change  $\Delta I(A_n; B_n)$ , with contours running downwards from  $0.3$  in units of  $0.1$ . (c) Free-energy change in tape  $A$ ,  $\Delta \tilde{F}(A_n)$ , with contours running upwards from  $0k_B T$  in units of  $0.1k_B T$ . (d) Change in the combined free energy of both tapes  $\Delta \tilde{F}(A_n, B_n)$ , with contours running downwards from  $1k_B T$  in units of  $0.1k_B T$ . In all cases, solid contours indicate  $0$ , dotted contours are positive values and dashed contours are negative. Note that although distorted compared to Fig. 8, the overall behaviour is very similar.

Similarly, the work done on the chemical bath contains a term due to the intrinsic stability of ATP and ADP

$$\langle w_{\text{cycle}} \rangle = (q - p_{\tau}(A_n = X^*)) \left( \Delta F_{\text{D} \rightarrow \text{T}}^0 + k_B T \ln \left( \frac{1 + \alpha}{1 - \alpha} \right) \right) \quad (\text{C4})$$

The time evolution of the system can be solved exactly as in Section B, and equivalent quantities are required to calculate  $\Delta I(A_n; B_n)$ ,  $\langle w_{\text{cycle}} \rangle$ ,  $\Delta \tilde{F}(A_n)$  and  $\Delta \tilde{F}(A_n, B_n)$ . We plot these quantities as a function of  $\alpha$  and  $\psi$  for  $q = 0.7$  in Fig. 9, with the rate constants specified in the caption. Although the shape is distorted, the regimes and dividing lines identified in our earlier analysis still appear. Indeed, the only qualitative difference between Fig. 8 and Fig. 9 is that the contour  $0_d$  (a line along which  $\Delta \tilde{F}(A_n) = 0$ ), now appears on the top right rather than the bottom left of the figure. In the new setting, inverting the probabilities of  $X$  and  $X^*$  does not preserve  $\tilde{F}(A_n)$ , since  $X$  and  $X^*$  have different intrinsic stabilities. In fact, for the parameters we have chosen,

$X^*$  is more stable than  $X$ . Therefore the line  $0_d$ , with  $\Delta \tilde{F}(A_n) = 0$ , is found at an even larger excess of  $X^*$  than initially, with the decrease in  $H(A)$  compensated by the increased intrinsic stability of molecules attached to tape  $A$ .

Importantly, even with unequal rates, the existence of mutual information between  $A$  and  $B$  always implies a thermodynamic resource  $k_B T I(A_n; B_n)$  that can be exploited. It is also always possible to chose a value of  $q$  such that  $\tilde{F}(A_n) = F_{\text{eq}}(A_n)$ , and the information is the only resource of the tapes. For our parameters in Fig. 9, this value is  $q \approx 0.82$ . By contrast, the “information entropy”  $H(A_n)$  that is exploited in many other hypothetical machines [21–23] has a less important role when rate constants are varied. In particular,  $H(A_n) < H_{\text{max}}(A_n)$  does not necessarily imply a reservoir from which work can be extracted, and tape  $A$  can either increase or decrease  $H(A)$  as it does work on its environment.

## Appendix D: Explicit verification of fluctuation relations during $\tau$

Trajectories  $z(t) = (e(t), a_n(t), b_n(t))$  within the window  $0 \rightarrow \tau$  generate a stochastic entropy  $\sigma[z(t), p_t(z)]$  that has two contributions: one from the details of trajectory itself and another from the overall evolution of the probability distribution of the system,  $p_t(z)$  [41, 43].

$$\sigma[z(t), p_t(z)] = k_B \ln \frac{p[z(t)|z_0]}{p^*[z^*(t)|z_\tau]} - k_B \ln \frac{p_\tau(z_\tau)}{p_0(z_0)}, \quad (\text{D1})$$

where  $p^*[z^*(t)|z_\tau]$  is the probability of the time-reversed trajectory occurring under time-reversed protocols, given a starting point equal to the end-point of the forward trajectory  $z_\tau$ . The first term can be further subdivided into [42, 43]

$$k_B \ln \frac{p[z(t)|z_0]}{p^*[z^*(t)|z_\tau]} = -\frac{Q_{\text{in}}}{T} + \Delta s_{0,\tau}^{\text{int}}, \quad (\text{D2})$$

where  $Q_{\text{in}}$  is the total heat input to the combined enzyme, tape and bath system, and  $\Delta s_{0,\tau}^{\text{int}}$  is the increase in intrinsic entropy of the states of the enzyme, tapes and bath between the initial and final states. The intrinsic entropy is a property of the chemical macrostate, and arises from coarse graining [42].

The absence of a time-dependent control means that  $Q_{\text{in}}$  is given solely by the change in internal energy of the combined system of enzymes, tape and bath,  $\Delta \mathcal{E}_{0,\tau}$ . Thus in this special case, the entropy generated by  $z(t)$  is specified purely by the initial and final states of the system

$$\sigma[z(t), p_t(z)] = -\frac{\Delta \mathcal{E}_{0,\tau}}{T} + \Delta s_{0,\tau}^{\text{int}} - k_B \ln \frac{p_\tau(z_\tau)}{p_0(z_0)}, \quad (\text{D3})$$

As a consequence, the fluctuation relation  $\langle \exp(-\sigma[z(t), p_t(z)]/k_B) \rangle = 1$  can be verified simply by summing  $\exp(-\sigma[z(t), p_t(z)]/k_B)$  over all possible combinations of initial and final states, weighted by the probabilities of those combinations occurring (which follow from the solution of the system in Section B). As noted in the main text, in our case this fluctuation relation is equivalent to  $\langle e^{-\bar{\sigma}[e_n(t), a_n(t), p_t(e, a_n)]/k_B + \Delta i_{0,\tau}(b_n; e, a_n)} \rangle = 1$  [17], where  $i(b_n; e, a_n) = \ln(p(b_n, e, a_n)/p(b_n)p(e, a_n))$  is the pointwise mutual information between  $B_n$  and  $A_n, E$  and

$$\bar{\sigma}[e_n(t), a_n(t), p_t(e, a_n)] = -\frac{\Delta \mathcal{E}_{0,\tau}}{T} + \Delta s_{0,\tau}^{\text{int}} - k_B \ln \frac{p_\tau(e_\tau, a_{n\tau})}{p_0(e_0, a_{n0})} \quad (\text{D4})$$

is the entropy change due to reactions involving  $E, A_n$  and the chemical bath. This relation holds since

$$k \ln \frac{p_\tau(z_\tau)}{p_0(z_0)} = k_B \ln \frac{p_\tau(e_\tau, a_{n\tau})}{p_0(e_0, a_{n0})} + k_B \Delta i_{0,\tau}(b_n; e, a_n), \quad (\text{D5})$$

noting that  $B_n$  does not change during the dynamics

There are 12 possible initial states and 12 possible final states to sum over. The dynamics does not connect initial and final states with different  $B_n$ , which leaves 72 distinct combinations of initial and final states. Further, states of different  $A_n$  and  $B_n = \bar{Y}$  are unconnected, leaving only 54 combinations, which can be trivially summed over using *eg.* Mathematica to demonstrate that  $\langle \exp(-\sigma[z(t), p_t(z)]/k_B) \rangle = \langle e^{-\bar{\sigma}[e_n(t), a_n(t), p_t(e, a_n)]/k_B + \Delta i_{0,\tau}(b_n; e, a_n)} \rangle = 1$ .

For the case of infinite  $\tau$ , and assuming that manipulation of the tapes is performed quasistatically, this is the only entropy generation from the system during operation. For finite  $\tau$ , the enzyme relaxes after the interaction window, the fluctuation theorem for which can also be verified explicitly.

## Appendix E: Subtleties relating to external manipulation of the tapes

The operation of the device requires the tapes to be slowly moved past the enzyme. This could be done continuously, or in stages (move, stop, move again). In either case the modelling of the interactions as constant for a fixed time  $\tau$  is only approximate, although it is unlikely that lifting this approximation would provide fundamentally different physics.

If the tapes are pulled at a finite rate, work will be done in the attachment/detachment of proteins as they move past the enzyme that is not included in our analysis. This is particularly true for the  $Y - E$  interaction, which is assumed to be reasonably strong. If this dissipation is to be minimised through slow manipulation of the tapes, it sets requirements on the intrinsic stability of the phosphorylation states of  $X$  as well as the DNA structure (as does the construction process). We note that these requirements are only evident when the interaction between information and the device is made physical, as in this case but not in prior work .

As has been argued elsewhere, infinitely slow but unidirectional motion implies finite dissipation when the system that causes unidirectional motion is taken into account [44]. If multiple tapes are manipulated simultaneously, however, this required dissipation does not scale extensively with the system size. Although in principle forces can be applied to biochemical systems using, for example, electric fields, in practice manipulation is often achieved using devices such as optical tweezers. In this case the manipulating device is enormously dissipative, a factor that is usually neglected. The possibility of eliminating this dissipation, along with the need to manipulate tapes slowly and the consequent requirements for stability of the system, make autonomous devices attractive.

## Appendix F: Subtleties related to averaging the mutual information over trajectories

In the main text we introduced an autonomous device that could interact with a number of  $(A_n, B_n)$  pairs without being manipulated. In Fig. 3c we plotted the time evolution of the mutual information between pairs of sites, obtained by averaging  $p_t(a_n, b_n)$ ,  $p_t(a_n)$  and  $p_t(b_n)$  over multiple simulations and then calculating  $I(A_n; B_n)$ . Also shown are the values of  $I(A_n; B_n)$  obtained within individual stochastic simulations, calculated by estimating  $p_t(a_n, b_n)$ ,  $p_t(a_n)$  and  $p_t(b_n)$  by sampling from many equivalent pairs of sites within state  $z(t)$  of the simulation, and identifying *e.g.*  $p_t(a_n)$  as the fraction of  $A$  in state  $X^*$  at time  $t$ .

Formally, although the estimates in the second case have means equal to  $p_t(a_n, b_n)$ ,  $p_t(a_n)$  and  $p_t(b_n)$  respec-

tively, their fluctuations about the means are correlated. Thus averaging the apparent mutual information – a non-linear function of probabilities – in each individual simulation does not give the true mutual information between  $A_n$  and  $B_n$ .  $I(A_n; B_n)$  is the physically meaningful quantity from which work can be extracted, since the average of the trajectory-dependent information associates information with random fluctuations in equilibrium, which of course could only be exploited through additional measurement and correlation.

This subtlety does not arise for the work, for which the physically meaningful quantity is the average of the work obtained in each individual simulation. In practice, however, we observe that the differences between the average of the trajectory-dependent information and the true  $I(A_n; B_n)$  are relatively small unless  $I(A_n; B_n) \approx 0$  or the total number of pairs is very low.